Peripheral circuits for ideal performance of a traveling-wave parametric amplifier

Hampus Renberg Nilsson,* Daryoush Shiri, Robert Rehammar, Anita Fadavi Roudsari, and Per Delsing

Department of Microtechnology and Nanoscience—MC2, Chalmers University of Technology, Göteborg S-412 96, Sweden

(Received 31 January 2024; revised 11 April 2024; accepted 6 June 2024; published 26 June 2024)

We investigate the peripheral circuits required to enable ideal performance for a high-gain traveling-wave parametric amplifier (TWPA) based on three-wave mixing . By embedding the TWPA in a network of superconducting diplexers, hybrid couplers, and impedance matching networks, the amplifier can deliver a high stable gain with near-quantum-limited noise performance, with suppressed gain ripples, while eliminating the reflections of the signal, the idler and the pump as well as the transmission of all unwanted tones. We also demonstrate a configuration where the amplifier can isolate. We call this technique *wideband idler filtering* (WIF). The theory is supported by simulations that predict over 20 dB gain in the 4–8 GHz band with 10 dB isolation for a single amplifier and 30 dB isolation for two cascaded amplifiers. We demonstrate how the WIF-TWPAs can be used to construct controllable isolators with over 40 dB isolation over the full 4–8 GHz band. Finally, we look at nonidealities and show how certain nonidealities can be devastating for both the gain and the idler filtering, especially a cutoff imbalance or a flux imbalance, and discuss how to compensate for them.

DOI: 10.1103/PhysRevApplied.21.064062

I. INTRODUCTION

To build large-scale multiqubit quantum processors, quantum-limited amplifiers [1] with high gain are desired. They are typically built with superconducting lumped-element oscillators or transmission-line resonators and have demonstrated high gain with near-quantum-limited noise performance [2–6], becoming an essential part of the circuit quantum electrodynamics [7] toolbox. While Josephson parametric amplifiers show high gain and near-quantum-limited noise performance [8–16], they have a gain-bandwidth product limit which prevents the bandwidth from being large enough for multiplexing many qubits in large-scale quantum processors. Such a capability is provided by traveling-wave parametric amplifiers (TWPAs) [17–19] in which the gain-bandwidth product limit is relaxed.

The basic amplification principle of the TWPA is based on the interaction between a weak signal and a strong copropagating wave, called the pump, when propagating through a nonlinear medium. Under a certain phase-matching condition, this can result in spatially exponential growth of the signal amplitude while also generating another tone, the idler. In the quantum regime, the TWPA can also generate the quantum phenomenon of photon entanglement [20] and, under certain conditions, signal squeezing [21], i.e., phase-sensitive amplification.

There are essentially two different kinds of TWPAs: the kinetic inductance TWPA (KITWPA) which uses the nonlinear kinetic inductance of a superconducting transmission line [22–29], and the Josephson TWPA (JTWPA) which uses the nonlinear inductance of Josephson junctions [20,30–40]. TWPAs are further distinguished by what mixing process of microwave photons they implement, three-wave mixing (3WM) or four-wave mixing (4WM), as well as what kind of dispersion they use, typically resonant phase matching (RPM) [31,32] or periodic modulation [41]. In this paper we will focus on an RPM-based JTWPA implementing 3WM, as outlined in our previous work [42]. However, the theory is also applicable to other kinds of TWPAs.

The ideal low-noise amplifier should meet several criteria. It provides a large bandwidth with high gain and quantum-limited noise performance and only outputs the desired signal. It has minimal back-action on the signal sources, especially when the signal sources

*Contact author: Hampus.Renberg.Nilsson@chalmers.se

are sensitive quantum systems such as qubits. To prevent back-propagation of noise and other tones from what comes after the amplifier, isolation is often a desired property of the amplifier. This is usually solved by placing ferrite circulators [43] after the amplifier. To get rid of the back-action on the signal sources, ferrite circulators are usually also placed before the amplifier. While circulators work well on a small scale, they are not suitable on a large scale as they are magnetic and bulky devices. To be able to build large-scale quantum computers, we would hence greatly benefit from a wideband quantum-limited amplifier that both isolates on its own, while not outputting any unwanted tones. There have been previous works about nonreciprocal quantum-limited amplifiers, but they typically do not have a large bandwidth [44,45] or they require a second parametric process [46–48]. There are also other properties that may be desired, such as a high saturation power, ease of use, scalability, robustness to stray magnetic fields, etc., which are outside the scope of this paper.

In this paper, we investigate how to build a near-quantum-limited amplifier which, in many ways, is the ideal low-noise amplifier. By embedding the amplifier in a network of diplexers and hybrid couplers, we eliminate all reflections and create isolation, while only outputting one signal for each signal input.

II. THREE-WAVE MIXING: PHASE MATCHING, UP-CONVERSION AND IMPEDANCE MATCHING

The theory in the next sections is valid for all 3WM amplifiers, but all numbers presented are based on a particular design from our previous work [42]. In this section we briefly go through the basics of 3WM, the necessities of phase matching while suppressing up-conversion, as well as impedance matching.

Three-wave mixing is a three-photon process, where either one photon down-converts into two other photons, $\omega_3 \mapsto \omega_1 + \omega_2$, or two photons up-convert into a third photon, $\omega_1 + \omega_2 \mapsto \omega_3$. The desired process in a 3WM amplifier is the down-conversion of the pump to a signal and an idler, $\omega_{p\mapsto}\omega_{s+}\omega_i$. However, it has previously been shown that 3WM also supports several undesired up-conversion processes [49], such as up-conversion of the signal, $\omega_{s+}\omega_{p\mapsto}\omega_{s+p}$. These up-conversion processes deteriorate the gain as they transfer power to other frequencies depleting the pump, the signal, and the idler. This, in turn, causes the inherently small phase mismatch to have a worse impact than previously believed. We showed in our previous work [42] that due to these up-conversion processes, 3WM cannot have exponential gain without dispersion engineering, as either phase mismatch or up-conversion processes, or both, will prevent it.

Due to the similarities between the TWPA structure and a low-pass filter, the TWPA has an intrinsic cutoff frequency. Thus, ideally no frequencies above the cutoff frequency can enter the TWPA. Moreover, there is a large dispersion for frequencies close to the cutoff frequency. To enable exponential gain, one has to work with a cutoff frequency either much larger than the signal frequencies to get phase matching while using dispersion engineering to suppress the up-conversion processes [41], or close to the signal frequencies to suppress the up-conversion processes while using dispersion engineering to get phase matching [42]. In this paper we will focus on the latter as it provides the highest gain per unit cell.

The TWPA in this study consists of 100 cascaded unit cells. The unit cell is presented in Fig. 1(a). The line inductance, as well as the nonlinear inductor enabling 3WM, is provided by a superconducting nonlinear asymmetric inductive element (SNAIL) [50], biased by a magnetic dc flux such that it provides pure 3WM and no 4WM or Kerr effect. The SNAIL consists of a superconducting loop with several Josephson junctions, in this study two junctions, in one arm with a critical current I_c, and a single Josephson junction in the other arm with a critical current αI_c, where $\alpha \leq 1$; in this study $\alpha = 0.44$. The ground capacitance is provided by the RPM feature consisting of a capacitor C in parallel with a capacitively coupled LC oscillator with inductance L_{osc}, capacitance C_{osc} and coupling capacitance C_c, as outlined in Refs. [31,32].

The key difference between the TWPA in Ref. [32] and the one presented here is that the cutoff frequency here is much smaller, approximately 16 GHz, and the resonance of the RPM feature 11.8 GHz is *below* the pump frequency 12 GHz to ensure phase matching for the 3WM process. The RPM feature is only weakly coupled to the signal line, $C_c = C/10$ and $C_{\text{osc}} = C$, to ensure phase matching in a wide band. The lower frequencies are achieved by using larger capacitances, $C + C_c = 386$ fF, and smaller critical currents of the junctions, $I_c = 1$ μA.

Due to the asymmetry of the unit cell, the TWPA gets an asymmetric structure with an inductive side and a capacitive side; see Fig. 1(b). To improve impedance matching, half of the capacitance can be moved from the capacitive side to the inductive side to form a symmetric π-structure, or half of the inductance from the inductive side to the capacitive side to form a symmetric T-structure.

With this TWPA structure, all up-conversion processes inside the 4–8 GHz gain band are suppressed since both the lowest signal frequency plus the pump frequency is above the cutoff frequency, 4 GHz + 12 GHz = 16 GHz, and the smallest idler frequency 12 GHz − 8 GHz = 4 GHz plus the pump frequency is also above the cutoff frequency; see Fig. 1(c). At the same time, the resonance below the pump frequency ensures phase matching. This way, we get a large exponential gain [42].

The pump amplitude could be increased to a point of more than 40 dB gain before reaching the critical currents of the Josephson junctions inside the SNAIL. However, impedance matching issues will appear already at lower

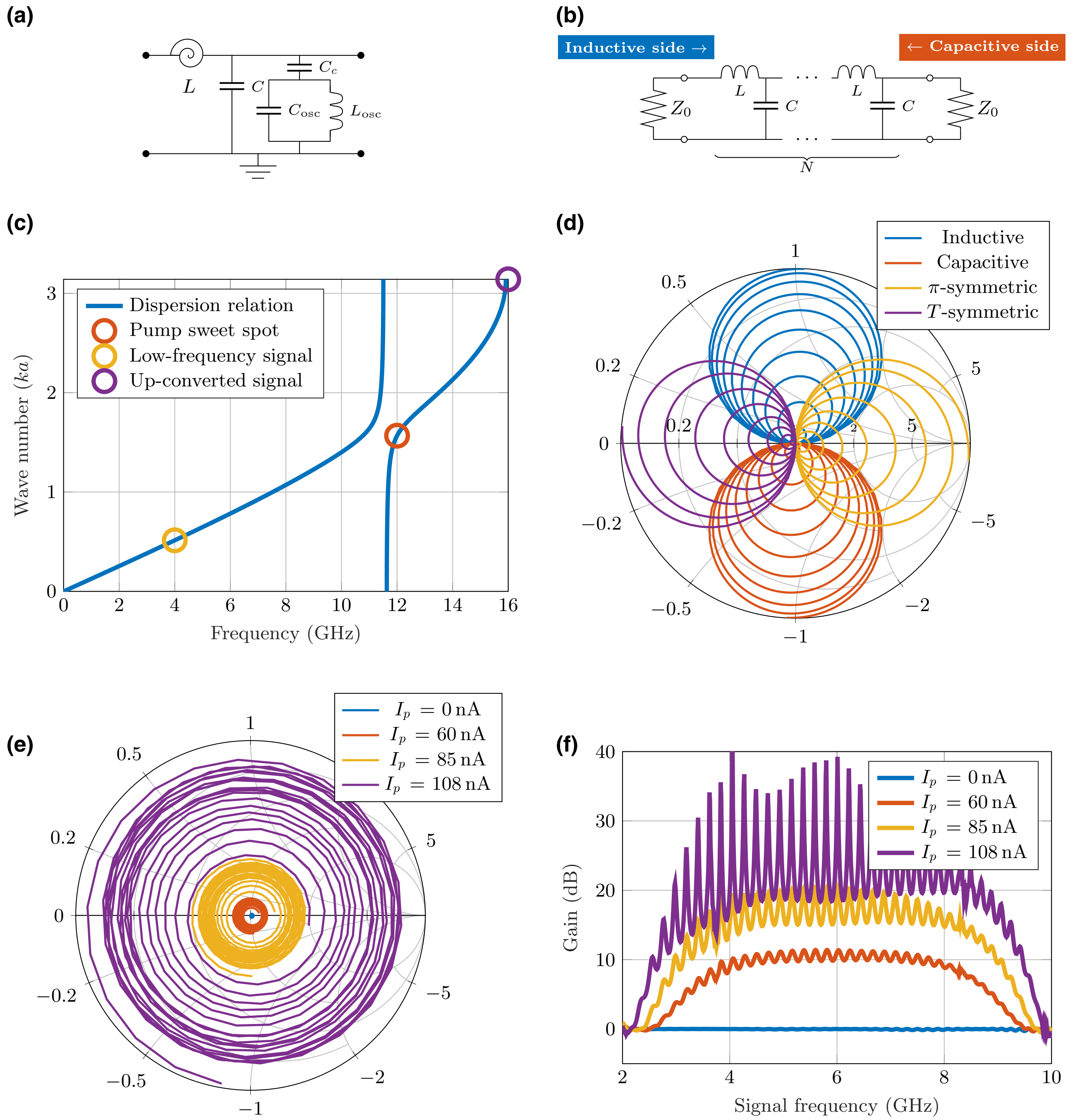

FIG. 1. The TWPA basics. (a) The TWPA unit cell with line inductance L, ground capacitance C, RPM coupling capacitance C_c, RPM oscillator capacitance C_{osc}, and RPM oscillator inductance L_{osc}. (b) The asymmetric LC chain. (c) The wave number k times the unit cell length a as a function of frequency with a small signal frequency (yellow), the pump frequency (orange), and the up-converted signal frequency (purple) shown. (d) The reflection coefficient of a discrete LC chain with $N = 10$ unit cells for frequencies from zero up to the cutoff frequency (16 GHz) for the asymmetric (blue and orange) and symmetric (yellow and purple) chains. (e) Simulated reflection coefficient in the 4–8 GHz band of the TWPA model, built from 100 unit cells [see (a)], for $I_p = 0\,\text{nA}$ (blue), $I_p = 60\,\text{nA}$ (orange), $I_p = 85$ nA (yellow), and $I_p = 108$ nA (purple). (f) Simulated gain of the same TWPA model and the same pump strengths as in (e).

power levels and thus be the limiting factor. When connecting the TWPA input and output ports to a 50-Ω environment, reflections will occur at the ports due to the complex and frequency-dependent impedance of the TWPA. In Fig. 1(d) we present the reflection coefficient for 10 unit cells of both the asymmetric and symmetric

LC chains, which is very similar to the impedance of our TWPA model except for frequencies close to the resonance of the RPM feature. These reflections will in turn make the amplifier unstable.

To mitigate the issue of impedance mismatch we add impedance matching networks to the input and output ports of the TWPA. The impedance matching networks are built as a chain of symmetric π-cells, but with smaller and varying values for the inductances and capacitances, chosen and tuned such that the reflections become small [51]. While they do not make the TWPA perfectly impedance matched, the reflections can be made negligibly small; see the blue dot in the middle of Fig. 1(e). However, when the pump is on and its amplitude turned up there is a new kind of impedance mismatch occurring, compare the different curves in Fig. 1(e). As can be seen, the TWPA is impedance matched at small pump currents, but not at larger ones. This gives rise to gain ripples; see Fig. 1(f). The same phenomenon also gives rise to signal reflection, which can be problematic since the reflections occur at the exact frequency of the signal source.

Note that the reflection coefficient in Fig. 1(e) is symmetric around the origin, unlike the reflection coefficient in Fig. 1(d), meaning we can no longer solve this impedance mismatch with impedance matching networks. In Sec. III we will look at more complicated techniques to solve this issue.

The reflection coefficient and the gain presented in Figs. 1(e) and 1(f), as well as all later figures of the reflection coefficients and gains, are simulated using harmonic balance in Keysight PathWave Advanced Design System. We built a nonlinear model for the Josephson junctions and the SNAIL [52], similarly to the works on KITWPAs [53], and simulated the transmission and reflection of the pump, signal, and idler.

To understand where this impedance mismatch comes from, it is instructive to look at the pumpistor model [54,55]. The model tells us that the generation of the idler gives a perturbation to the unit cell impedance which can be modeled as a complex-valued inductance, the "pumpistor". The imaginary part of this complex inductance is equivalent to a negative resistance, and this negative resistance of the pumpistor explains both the gain and the impedance mismatch. While the works on the pumpistor model were done for the flux-pumped TWPA, the same principles apply for the current-pumped TWPA which we use here.

In summary, by using a TWPA made with 100 cascaded unit cells of the structure shown in Fig. 1(a) and adding impedance matching networks to the input and output ports, we get an amplifier with a high gain in a wide band. This amplifier should ideally have a quantum-limited noise performance. However, it is not the ideal low-noise amplifier, as it also has a lot of reflections at high gain, it does not isolate, and it outputs the signal, the idler, and the pump. In Sec. III we will look at different peripheral circuits to address these issues.

III. THE SINGLE-LAYERED WIF-TWPA

In Sec. II we saw that, while the unpumped TWPA is impedance matched, the pumped TWPA is not, which gives rise to large gain ripples and signal reflections. Furthermore, the reflection coefficient is symmetrically rotating around the origin of the Smith chart, meaning we cannot solve this issue with more impedance matching networks. In this section we will look at other, more complicated, techniques to get rid of these reflections and this impedance mismatch, as well as how to get rid of pump and idler leakage.

The usual way to get rid of the signal reflections is with the use of ferrite circulators. However, as mentioned previously, it is not easy to scale up such a solution since ferrite circulators are bulky and magnetic devices and space is a limited resource in the cryostats where these amplifiers are used. Here we instead propose to build a balanced TWPA [56], i.e., two identical TWPAs in parallel connected to each other via 90° hybrid couplers; see Fig. 2(a). This ensures that the reflections of the two TWPAs destructively interfere towards the input port, and hence that the device remains impedance matched. Meanwhile, assuming that the 50-Ω terminations, depicted in the figure as squares with small resistors inside, are thermally well anchored to the environment, they will not add any noise apart from quantum noise.

Another issue with TWPAs is the leakage of the pump, both forwards towards the next amplifier and backwards towards the signal source. In most works, the pump has been coupled to the signal line via a directional coupler. While this works for the purpose of coupling the pump, it does not prevent the reflected portion of the pump from traveling towards the signal source, nor does it prevent the transmitted portion of the pump from traveling with the signal towards the next amplifier. Due to finite directivity, the directional coupler will also transmit a portion of the pump in the direction of the signal source. Another solution for coupling the pump is adding diplexers [51] in front of and after the TWPA; see Fig. 2(b). A diplexer both couples the pump and filters out the reflection portion of the pump. Since the pump frequency for 3WM is typically around twice that of the signal, there is plenty of playroom for the diplexers to filter the pump. Specifically in our case, we aim to amplify the 4–8 GHz band. Hence, the pump should be around 12 GHz, so we use superconducting diplexers with a transition frequency of 9 GHz.

The balanced TWPA solves the issue of signal reflection, and the diplexed TWPA ideally suppresses the pump leakage completely. The most straightforward way to connect them is to connect the diplexers to the balanced amplifier; see Fig. 2(c). Assuming identical TWPAs, ideal

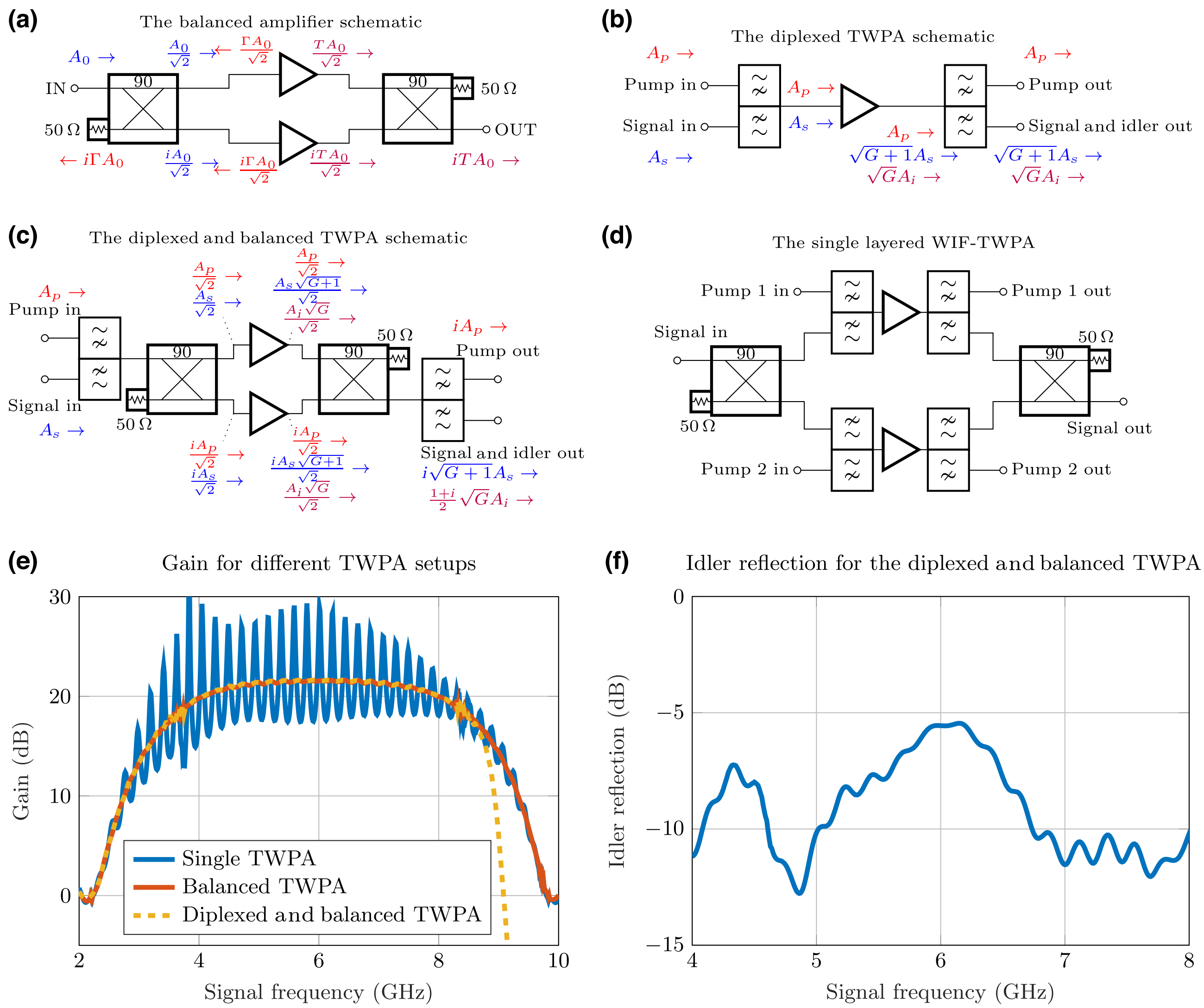

FIG. 2. Different TWPA peripheral circuits. (a) A balanced amplifier setup with the incoming wave (blue), the reflected wave (red), and the transmitted wave (purple). (b) A diplexed TWPA with the transmission of the pump (red), the signal (blue), and the idler (purple). (c) A diplexed and balanced TWPA. (d) The single-layered WIF-TWPA. (e) Simulated gain profiles of the TWPA with the different peripheral circuits for $I_p = 100$ nA. (f) The idler reflection in relation to the initial signal amplitude at the "signal in" port of the balanced and diplexed TWPA in the 4–8 GHz band for $I_p = 100$ nA.

hybrid couplers and diplexers, we have now eliminated all signal reflection and all pump leakage. The simulated gain for the single TWPA, the balanced TWPA [Fig. 2(a)], and a balanced TWPA with 9 GHz transition frequency diplexers [Fig. 2(c)] is presented in Fig. 2(e). In the simulation we have used ideal hybrid couplers [57], i.e., couplers with perfect amplitude and phase balance in the full frequency band, and 11th-order Chebyshev diplexers with 0.1 dB ripples.

As can be seen in Fig. 2(e), balancing the TWPA solves the issue of gain ripples, and adding the diplexers only affects the gain when approaching the diplexer transition frequency of 9 GHz. If one does not want to lose any gain bandwidth, one can move the diplexer transition frequency to a higher frequency (e.g., 10 GHz), but that would make it more challenging to sufficiently filter out the pump.

The setup presented in Fig. 2(c) does not, however, resolve the issue of idler leakage. As shown in Fig. 2(f), a part of the reflected idler still leaks backwards towards the signal source. The issue comes from the fact that the idler phase for 3WM is given by $\phi_i = \phi_p - \phi_s$ [19]. Both the pump and the signal phases increase by 90° in the lower branch of the balancing scheme in Fig. 2(c), hence canceling out their effects on the idler phase. Therefore, the idler in the lower branch of Fig. 2(c) will be in phase with the idler in the upper branch, and once it reaches the hybrid couplers, half of the reflected idler will leak through the left coupler in Fig. 2(c) and half of the transmitted idler will leak through the right coupler in Fig. 2(c).

To be able to suppress the idler leakage, we must instead make a balanced amplifier with two diplexed amplifiers; see Fig. 2(d). This design we refer to as the (single-layered) *wideband idler filtering* (WIF) TWPA. While this new setup requires two pump inputs, similar to the multipath interferometric Josephson directional amplifier [45], it also gives an added degree of freedom: the phase difference $\Delta\phi_p = \phi_{p2} - \phi_{p1}$ between the pumps.

If the pumps are in phase with each other (i.e., $\Delta\phi_p = 0$), all of the transmitted idler goes into the right 50-Ω termination in Fig. 2(d). By swapping the "signal out" with the right termination and reading out at the idler frequency, we get an isolating amplifier since any wave entering at the output port would end up in the left termination. However, this solution does not suppress the idler reflections.

If the pumps are out of phase with each other (i.e., $\Delta\phi_p = \pi$), all of the reflected idler goes into the left 50-Ω termination in Fig. 2(d). However, this solution does not separate the transmitted idler from the transmitted signal, and hence cannot isolate the input from the output.

To solve all these issues simultaneously, we need to use a more complicated setup, which we will outline in Sec. IV.

IV. THE DOUBLE-LAYERED WIF-TWPA

While the single-layered WIF-TWPA [recall Fig. 2(d)] suffices when the amplifier user does not need isolation or when idler reflections are tolerable, it is not good enough for all applications as it cannot filter both the reflected and the transmitted idler *simultaneously*. Here we propose a modified version that can do just that, the double-layered WIF-TWPA. It consists of two single-layered WIF-TWPAs in parallel, connected to each other via another layer of hybrid couplers; see Fig. 3(a). This gives us one signal input, one signal output, one idler output, four pump inputs, and four pump outputs, and provides three degrees of freedom: the phases of the second,

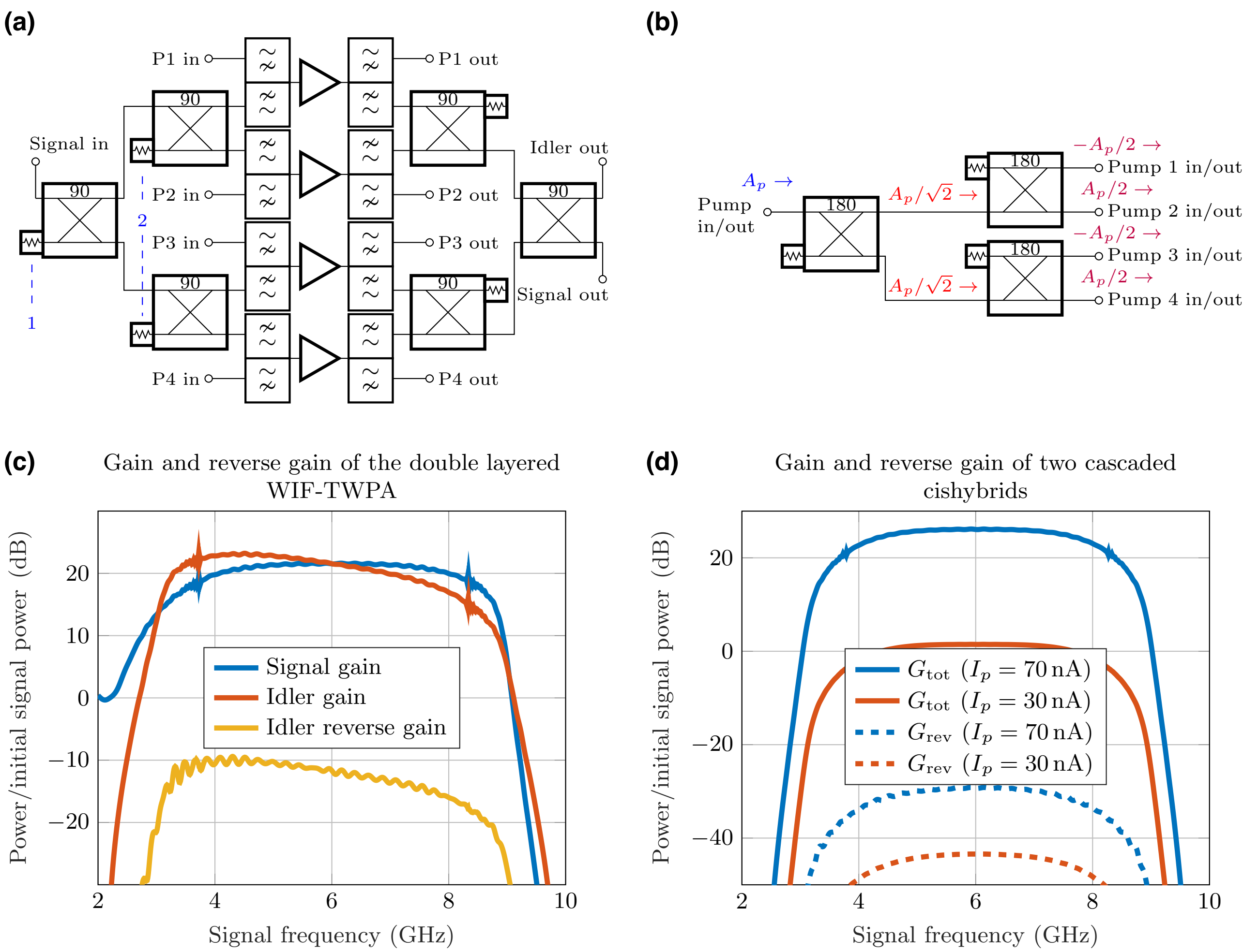

FIG. 3. The double-layered WIF-TWPA. (a) Schematics of the double-layered WIF-TWPA. (b) A network of couplers creating the desired pump phases of Eq. (1). (c) Simulated signal gain, idler gain, and reverse idler gain of a double-layered WIF-TWPA. (d) Simulated total gain $G_{\rm tot}$ and reverse gain $G_{\rm rev}$ for two cascaded double-layered WIF-TWPAs.

third, and fourth pumps ($\phi_{p2}, \phi_{p3}, \phi_{p4}$) in relation to the first (ϕ_{p1}).

Here we will focus on one combination in particular:

$$\phi_{p2} = \phi_{p4} = \phi_{p1} + \pi = \phi_{p3} + \pi. \quad (1)$$

These pump phases can be generated by using four different phase-locked signal sources and setting the phases manually. A more convenient way, however, is to use three 180° hybrid couplers, similar to a Butler matrix [58] [see Fig. 3(b)], which are connected to each side of the double-layered WIF-TWPA.

With this, we get a five-port device: The signal input, the signal output, the idler output, and only one pump input, "pump in" in Fig. 3(b), and one pump output, "pump out" in Fig. 3(b). This device can be connected in several different ways, giving different properties. With this setup, the pump is filtered out with the diplexers and the reflected signal and idler are terminated by the terminations labeled "2" in Fig. 3(a). The transmitted idler is fully separated from the transmitted signal and exits at the "idler out" port, while the signal exits at the "signal out" port.

If we now terminate the "idler out" port, we get an amplifier without any leakage. We refer to this as the "transhybrid" setup, as the signal path is similar to the shape of a transisomer of a molecule. However, any unwanted wave entering at the output port will be able to propagate through the amplifier and towards the sensitive signal sources. If we instead terminate the "signal out" port, any unwanted wave entering at the output is terminated at the termination labeled "1", hence giving isolation. The only drawback is that we now need to readout at the idler frequency instead of the signal frequency. We refer to this as the "cishybrid" setup, as the signal path is similar to the shape of a cisisomer of a molecule.

If we assume ideal components, the double-layered WIF-TWPA cishybrid has perfect isolation when it is not pumped. However, when we pump it, the isolation is reduced at the idler frequency due to a weak interaction between the incoming waves and the counterpropagating pump. The isolation reduction is dependent on the pump amplitude. When we pump it such that we get 20 dB gain, the isolation is reduced to only about 10 dB; see Fig. 3(c). In this figure, the "idler gain" refers to the power of the idler in relation to the initial signal power, the "signal gain" refers to the gain if we were to read out at the "signal out" port, and the "idler reverse gain" refers to the power of the idler, in relation to the initial signal power, generated by a signal entering at the "idler out" port.

To improve the isolation, and also retrieve the initial signal frequency, we can cascade two cishybrids; see Fig. 3(d). Then we will not only improve the isolation, but also retrieve the original signal frequency. If we only care about isolation and do not require any gain, we can pump more weakly, which improves the isolation. Note that this setup is symmetric, i.e., we can decide in which directions it should transmit and isolate by choosing the direction of the pump.

V. EFFECTS OF NONIDEALITIES

Until now, we have assumed that all components are ideal. In this section we will discuss the effects of nonidealities, first the effects of nonidealities in the peripheral circuitry, then the effects of nonidentical TWPAs. To simplify this analysis we will confine this study to the single-layered WIF-TWPA, shown in Fig. 2(d), with no pump phase difference ($\Delta\phi_p = 0$). For this device there should be no transmitted idler. We will therefore study the effects on the gain profile, as well as the leakage of the transmitted idler, to determine the impact of the different nonidealities.

A. Nonidealities in the peripheral circuitry

The peripheral circuitry can be nonideal in several ways. There may be amplitude or phase imbalances in the couplers and there may be amplitude or phase imbalances between the two inserted pumps. The imbalances between the pumps can come from several different sources: from the diplexers, from a power divider dividing a single pump into two, from the lines inserting the pumps, etc. The source of the imbalances is irrelevant for this analysis. In the simulations presented in this section, the pump imbalances will be simulated by using a nonideal 180° coupler.

Let us first consider imbalances in the output coupler, a phase imbalance $\Delta\phi_{\text{out}}$ or an amplitude imbalance ΔA_{out}. This will have no effect on the input impedance, and thus will not give rise to any ripples, but it will prevent the signal and idler from being fully separated at the output. With the simulated imbalances, we will barely lose any gain, but we will get some leakage of the transmitted idler at the output port; see the $\Delta\phi_{\text{out}}$ and ΔA_{out} curves in Figs. 4(a) and 4(b).

Let us next consider imbalances in the input coupler, a phase imbalance $\Delta\phi_{\text{in}}$ or an amplitude imbalance ΔA_{in}. These imbalances will both have a similar impact to imbalances in the output coupler, while also affecting the input impedance, and hence giving rise to some reflections and gain ripples; see the $\Delta\phi_{\text{in}}$ and ΔA_{in} curves in Figs. 4(a) and 4(b).

Note that the simulated imbalances in Figs. 4(a) and 4(b) are quite large, 1 dB and 5°, compared to the state-of-the-art values which are typically not larger than 0.3 dB and 2° [59].

Let us next consider a phase imbalance $\Delta\phi_p$ between the pumps. Since we are considering amplifiers implementing phase-insensitive amplification, the pump phases have no impact on the signal phase, and the gain profile for the signal is thus unaffected. They do, however, affect the idler

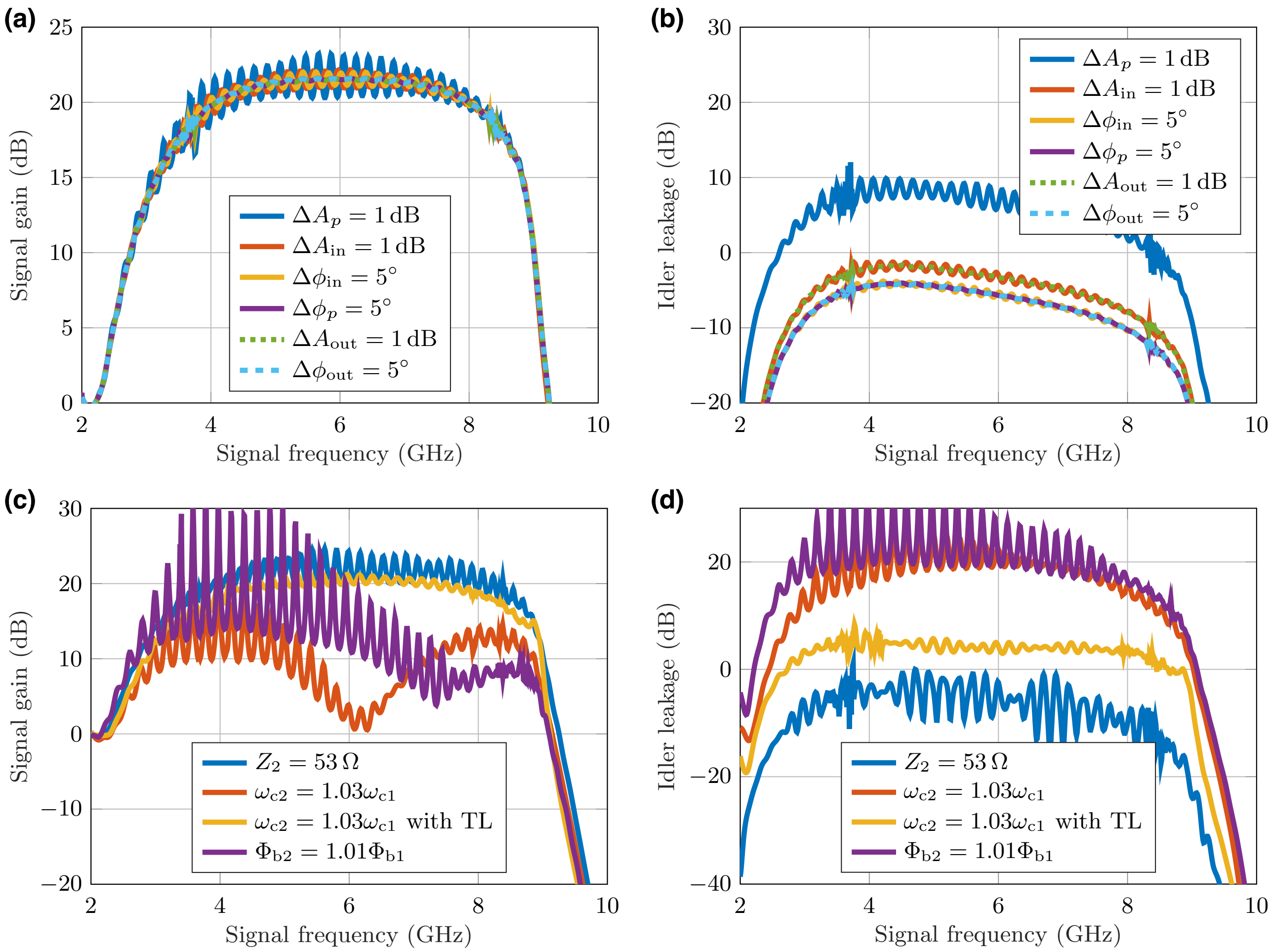

FIG. 4. The single-layered WIF-TWPA with nonidealities. (a) The signal gain for nonideal peripheral circuitry. (b) The idler leakage in relation to the initial signal amplitude for nonideal peripheral circuitry. (c) The signal gain for nonidentical TWPAs. (d) The idler leakage in relation to the initial signal amplitude for nonidentical TWPAs.

phase, which limits the ability of the WIF-TWPA to filter out the idler; see the $\Delta\phi_p$ curve in Fig. 4(b).

The effect on the idler leakage from $\Delta\phi_p$ is identical to that given by a phase imbalance $\Delta\phi_{\mathrm{out}}$ in the output coupler. We can hence compensate for the effects on the idler leakage of one of these imbalances with the other, i.e., by ensuring that $\Delta\phi_{\mathrm{out}} + \Delta\phi_p = 0$, there will be no idler leakage.

Finally, let us consider an amplitude imbalance between the pumps ΔA_p. This will make the two TWPAs have different amounts of gain and different reflection coefficients. This will hence give signal reflection, gain ripples, and idler leakage; see the ΔA_p curves in Figs. 4(a) and 4(b). Since the TWPAs are quite sensitive to the pump power, this is the issue that will give the largest deviations from ideal performance, given the assumed values of amplitude and phase imbalances we have used in this analysis. Fortunately, making a good power divider for the pump is a fairly simple task [57].

In conclusion, some imperfections in the peripheral circuitry are worse than others, but only a pump amplitude imbalance has a particularly large impact on the overall performance, and ensuring equal amplitudes of the two pumps is a relatively simple task.

B. Nonidentical TWPAs

Now let us discuss the effects of having nonidentical TWPAs. Each TWPA has 100 unit cells, and each unit cell has several inductors and capacitors. To simplify the analysis, we will assume that all inductors and capacitors have the desired relations between each other with a negligible spread, but that there may be an overall offset to them. This means that the TWPA impedance $Z = \sqrt{L/C}$ and/or the TWPA cutoff frequency $\omega_c \approx 2/\sqrt{LC}$ may have some shift.

Let us first consider an impedance imbalance between the TWPAs. More specifically, let us assume that the first

TWPA has the desired $Z_1 = 50\ \Omega$ impedance, while the second one has another impedance Z_2. Then the reflection coefficients will be different, resulting in gain ripples. The phase relation between the idler outputs will not be perfect, and induce some idler leakage; see the $Z_2 = 53\ \Omega$ curves in Figs. 4(c) and 4(d).

Let us next consider a cutoff frequency imbalance between the TWPAs. More specifically, let us assume that the first TWPA has the desired cutoff frequency of $f_{c1} \approx$ 16 GHz, while the second one has a larger cutoff frequency f_{c2}. As can be seen in the $\omega_{c2} = 1.03\omega_{c1}$ curves in Figs. 4(c) and 4(d), this has a much worse effect on the TWPA performance. It is easy to understand why. When changing the cutoff frequency, several things happen. To begin with, the sweet spot for the pump frequency shifts, so the gain goes down. This introduces amplitude imbalances between the signal and the idler. Secondly, the amount of phase per unit cell changes. While this change per unit cell is small, of the order of the ratio of the cutoff frequencies, the phase difference accumulates over the TWPAs. If the total phase difference becomes 180°, the output coupler will work fully counterproductively.

The latter of the two problems from a cutoff imbalance can be partially solved by adding a short transmission line in front of the low-pass port of the diplexer to the TWPA with the larger cutoff; see the "$\omega_{c2} = 1.03\omega_{c1}$ with TL" curves in Figs. 4(c) and 4(d). Here the "TL" refers to a transmission line with electrical length 160° at 6 GHz. Adding this transmission line helps since the transmission line adds the missing phase. This will not fully solve the issues introduced by the cutoff imbalance though, since the gains will still be different between the two TWPAs.

Finally, let us consider a flux-biasing difference. More specifically, let us assume that the first TWPA has the desired flux bias of $\Phi_{b1} = 0.43\Phi_0$, while the second one has a larger flux bias Φ_{b2}. Having different fluxes has a similar effect to having different cutoff frequencies [see the $\Phi_{b2} = 1.01\Phi_{b1}$ curves in Figs. 4(c) and 4(d)], since changing the flux bias changes the inductances and hence the cutoff. It also changes the mixing coefficients somewhat, which in turn changes the gain, but we expect this to be a minor problem compared to the cutoff imbalance.

In conclusion, among the issues of impedance imbalance and cutoff imbalance, the latter is far worse for TWPA performance. A flux imbalance has a similar devastating effect to a cutoff imbalance, so it is strongly advised to have independent flux lines for biasing each TWPA. While the issue of cutoff imbalance can be heavily suppressed by adding a short transmission line to the TWPA with the larger cutoff frequency, a more straightforward approach is to tune the flux biases such that there is only an impedance imbalance instead of a cutoff imbalance.

VI. DISCUSSION AND CONCLUSIONS

In this paper, we have discussed different issues with a high-gain traveling-wave parametric amplifier based on three-wave mixing, especially the lack of isolation and the leakage of unwanted tones both in the forward and backward directions, and we have proposed solutions to these problems: a peripheral circuit [60] for the TWPA to create what we call "wideband idler filtering" (WIF). In a regular TWPA, the pump can be filtered out by using diplexers, and signal reflection by building a balanced amplifier setup, but the idler reflection and the idler transmission are more difficult to filter without sacrificing bandwidth. We show that by putting the diplexers between the hybrid couplers and the two TWPAs in a balanced amplifier setup, and by setting the pump phases to appropriate values, either the reflected idler or the transmitted idler can be filtered out, but not both simultaneously. Then we show that by using four parallel TWPAs, coupling them to each other in a suitable way and setting the pump phases to appropriate values, we can filter out both the reflected and the transmitted idler and also achieve isolation. To further improve the isolation we can cascade two of these amplifiers. The different peripheral circuits and their capabilities are presented in Table I.

TABLE I. A summary of TWPA performance using the different peripheral circuits. The isolation numbers presented are for the approximately lowest isolation when our TWPA model delivers at least 20 dB gain in the full 4–8 GHz band.

	Signal reflection	Pump leakage	Idler leakage	Isolation
No peripheral circuits	Yes	Yes	Yes	0 dB
Balanced	No	Yes	Yes	0 dB
Diplexed	Yes	No	Yes	0 dB
Diplexed and balanced	No	No	Yes	0 dB
Single-layered WIF ($\Delta\phi_p = 0$)	No	No	Backwards	10 dB
Single-layered WIF ($\Delta\phi_p = \pi$)	No	No	Forwards	0 dB
Double-layered WIF (transhybrid)	No	No	No	0 dB
Double-layered WIF (cishybrid)	No	No	No	10 dB
Two cascaded cishybrids	No	No	No	30 dB
The ideal case	No	No	No	∞

We have also discussed different effects of different nonidealities. There can be nonidealities in the peripheral circuitry, and the TWPAs can be nonidentical. We have shown that nonidealities in the peripheral circuitry have a relatively small effect on performance, while nonidentical TWPAs have a much worse effect on performance. We also briefly discussed different ways of compensating for different nonidealities. A phase imbalance in the output coupler can be compensated for with the opposite phase imbalance between the pumps. A cutoff imbalance between the TWPAs can be compensated for, to an extent, by either adding a short transmission line or flux-tuning the TWPAs to instead have an impedance imbalance. A flux imbalance can be devastating and we therefore strongly recommend anyone implementing this technique to have separate flux lines to the TWPAs.

In conclusion, while the solutions presented in this paper may seem complicated, we want to stress that this essentially makes the ideal low-noise amplifier. It has, in theory, quantum-limited noise performance, a high gain, and a large bandwidth, while also both mitigating all leakage and providing isolation. Furthermore, since the hybrid couplers and the diplexers can be made much smaller than regular microwave isolators [61,62], and our TWPA design yields TWPAs with a very small number of unit cells, the complete setup presented in this paper has a much smaller footprint than typical TWPA setups today, making this setup a favorable one for large-scale quantum computers in the future. Other works on directional quantum-limited amplifiers typically do not have a large bandwidth [44,45], or require another parametric process [46–48]. The saturation power of our device, which is based on Josephson junctions, is not the largest, but the theory holds for all 3WM traveling-wave parametric amplifiers, including those based on kinetic inductance which typically have a higher saturation power. Since the amplifier isolates and only outputs one signal, while it does not reflect, it can be cascaded with other amplifiers to raise the saturation power. With small changes to the diplexers and the phase relations between the pumps, the theory also works for 4WM traveling-wave parametric amplifiers. In general, the ideas in this paper can be used for any amplifier that generates an idler.

ACKNOWLEDGMENTS

The project was supported by the Knut and Alice Wallenberg Foundation via the Wallenberg Centre for Quantum Technology. The authors would like to thank Vitaly Shumeiko for useful discussions leading to the TWPA model outlined in this paper, Christian Fager for assistance in setting up the simulation models, and Vincent Desmaris from GARD for sharing the specifications of their state-of-the-art hybrid couplers.

[1] C. M. Caves, Quantum limits on noise in linear amplifiers, Phys. Rev. D **26**, 1817 (1982).

[2] T. Yamamoto, K. Inomata, M. Watanabe, K. Matsuba, T. Miyazaki, W. D. Oliver, Y. Nakamura, and J. S. Tsai, Flux-driven Josephson parametric amplifier, Appl. Phys. Lett. **93**, 042510 (2008).

[3] N. Bergeal, F. Schackert, M. Metcalfe, R. Vijay, V. E. Manucharyan, L. Frunzio, D. E. Prober, R. J. Schoelkopf, S. M. Girvin, and M. H. Devoret, Phase-preserving amplification near the quantum limit with a Josephson ring modulator, Nature **465**, 64 (2010).

[4] N. Roch, E. Flurin, F. Nguyen, P. Morfin, P. Campagne-Ibarcq, M. H. Devoret, B. Huard, and Widely Tunable, Nondegenerate three-wave mixing microwave device operating near the quantum limit, Phys. Rev. Lett. **108**, 147701 (2012).

[5] A. Roy and M. Devoret, Introduction to parametric amplification of quantum signals with Josephson circuits, C. R. Phys. **17**, 740 (2016).

[6] J. Aumentado, Superconducting parametric amplifiers (review), IEEE Microw. Mag. **21**, 45 (2020).

[7] R. J. Schoelkopf and S. M. Girvin, Wiring up quantum systems, Nature **451**, 664 (2008).

[8] H. Zimmer, Parametric amplification of microwaves in superconducting Josephson tunnel junctions, Appl. Phys. Lett. **10**, 193 (1967).

[9] H. Kanter and A. H. Silver, Self-pumped Josephson parametric amplification, Appl. Phys. Lett. **19**, 515 (1971).

[10] M. J. Feldman, P. T. Parrish, and R. Y. Chiao, Parametric amplification by unbiased Josephson junctions, J. Appl. Phys. **46**, 4031 (1975).

[11] B. Yurke, P. G. Kaminsky, R. E. Miller, E. A. Whittaker, A. D. Smith, A. H. Silver, and R. W. Simon, Observation of 4.2-K equilibrium-noise squeezing via a Josephson-parametric amplifier, Phys. Rev. Lett. **60**, 764 (1988).

[12] B. Yurke, L. R. Corruccini, P. G. Kaminsky, L. W. Rupp, A. D. Smith, A. H. Silver, R. W. Simon, and E. A. Whittaker, Observation of parametric amplification and deamplification in a Josephson parametric amplifier, Phys. Rev. A **39**, 2519 (1989).

[13] H. K. Olsson and T. Claeson, Low-noise Josephson parametric amplification and oscillations at 9 GHz, J. Appl. Phys. **64**, 5234 (1988).

[14] M. A. Castellanos-Beltran, K. D. Irwin, G. C. Hilton, L. R. Vale, and K. W. Lehnert, Amplification and squeezing of quantum noise with a tunable Josephson metamaterial, Nat. Phys. **4**, 929 (2008).

[15] T. Roy, S. Kundu, M. Chand, A. M. Vadiraj, A. Ranadive, N. Nehra, M. P. Patankar, J. Aumentado, A. A. Clerk, and R. Vijay, Broadband parametric amplification with impedance engineering: Beyond the gain-bandwidth product, Appl. Phys. Lett. **107**, 262601 (2015).

[16] M. Simoen, C. W. S. Chang, P. Krantz, J. Bylander, W. Wustmann, V. Shumeiko, P. Delsing, and C. M. Wilson, Characterization of a multimode coplanar waveguide parametric amplifier, J. Appl. Phys. **118**, 154501 (2015).

[17] A. L. Cullen, A travelling-wave parametric amplifier, Nature (London) **181**, 332 (1958).

[18] P. K. Tien and H. Suhl, A traveling-wave ferromagnetic amplifier, Proc. Inst. Radio Eng. **46**, 700 (1958).

[19] P. K. Tien, Parametric amplification and frequency mixing in propagating circuits, J. Appl. Phys. **29**, 1347 (1958).

[20] M. R. Perelshtein, K. V. Petrovnin, V. Vesterinen, S. Hamedani Raja, I. Lilja, M. Will, A. Savin, S. Simbierowicz, R. N. Jabdaraghi, J. S. Lehtinen, L. Grönberg, J. Hassel, M. P. Prunnila, J. Govenius, G. S. Paraoanu, and P. J. Hakonen, Broadband continuous-variable entanglement generation using a Kerr-free Josephson metamaterial, Phys. Rev. Appl. **18**, 024063 (2022).

[21] A. L. Grimsmo and A. Blais, Squeezing and quantum state engineering with Josephson travelling wave amplifiers, npj Quantum Inf. **3**, 20 (2017).

[22] Byeong Ho Eom, Peter K. Day, Henry G. LeDuc, Jonas Zmuidzinas, and A. wideband, low-noise superconducting amplifier with high dynamic range, Nat. Phys. **8**, 623 (2012).

[23] C. Bockstiegel, J. Gao, M. R. Vissers, M. Sandberg, S. Chaudhuri, A. Sanders, L. R. Vale, K. D. Irwin, and D. P. Pappas, Development of a broadband NbTiN traveling wave parametric amplifier for MKID readout, J. Low Temp. Phys. **176**, 476 (2014).

[24] M. R. Vissers, R. P. Erickson, H.-S. Ku, Leila Vale, Xian Wu, G. C. Hilton, and D. P. Pappas, Low-noise kinetic inductance traveling-wave amplifier using three-wave mixing, Appl. Phys. Lett. **108**, 012601 (2016).

[25] S. Chaudhuri, D. Li, K. D. Irwin, C. Bockstiegel, J. Hubmayr, J. N. Ullom, M. R. Vissers, and J. Gao, Broadband parametric amplifiers based on nonlinear kinetic inductance artificial transmission lines, Appl. Phys. Lett. **110**, 152601 (2017).

[26] R. P. Erickson and D. P. Pappas, Theory of multiwave mixing within the superconducting kinetic-inductance traveling-wave amplifier, Phys. Rev. B **95**, 104506 (2017).

[27] S. Goldstein, N. Kirsh, E. Svetitsky, Y. Zamir, O. Hachmo, C. E. Mazzotti de Oliveira, and N. Katz, Four wave-mixing in a microstrip kinetic inductance travelling wave parametric amplifier, Appl. Phys. Lett. **116**, 152602 (2020).

[28] M. Malnou, M. R. Vissers, J. D. Wheeler, J. Aumentado, J. Hubmayr, J. N. Ullom, and J. Gao, Three-wave mixing kinetic inductance traveling-wave amplifier with near-quantum-limited noise performance, PRX Quantum **2**, 010302 (2021).

[29] D. J. Parker, M. Savytskyi, W. Vine, A. Laucht, T. Duty, A. Morello, A. L. Grimsmo, and J. J. Pla, Degenerate parametric amplification via three-wave mixing using kinetic inductance, Phys. Rev. Appl. **17**, 034064 (2022).

[30] O. Yaakobi, L. Friedland, C. Macklin, and I. Siddiqi, Parametric amplification in Josephson junction embedded transmission lines, Phys. Rev. B **87**, 144301 (2013).

[31] K. O'Brien, C. Macklin, I. Siddiqi., and Xiang Zhang, Resonant phase matching of Josephson junction traveling wave parametric amplifiers, Phys. Rev. Lett. **113**, 157001 (2014).

[32] C. Macklin, K. O'Brien, D. Hover, M. E. Schwartz, V. Bolkhovsky, X. Zhang, W. D. Oliver, and I. Siddiqi, A near-quantum-limited Josephson traveling wave parametric amplifier, Science **350**, 325 (2015).

[33] T. C. White, *et al.*, Traveling wave parametric amplifier with Josephson junctions using minimal resonator phase matching, Appl. Phys. Lett. **106**, 242601 (2015).

[34] M. T. Bell and A. Samolov, Traveling-wave parametric amplifier based on a chain of coupled asymmetric SQUIDs, Phys. Rev. Appl. **4**, 024014 (2015).

[35] L. Planat, A. Ranadive, R. Dassonneville, J. Puertas Martínez, S. Léger, C. Naud, O. Buisson, W. Hasch-Guichard, D. M. Basko, and N. Roch, Photonic-crystal Josephson traveling-wave parametric amplifier, Phys. Rev. X **10**, 021021 (2020).

[36] A. Ranadive, M. Esposito, L. Planat, E. Bonet, C. Naud, O. Buisson, W. Guichard, and N. Roch, Kerr reversal in Josephson meta-material and traveling wave parametric amplification, Nat. Commun. **13**, 1737 (2022).

[37] A. B. Zorin, Josephson traveling-wave parametric amplifier with three-wave mixing, Phys. Rev. Appl. **6**, 034006 (2016).

[38] A. B. Zorin, Flux-driven Josephson traveling-wave parametric amplifier, Phys. Rev. Appl. **12**, 044051 (2019).

[39] V. V. Sivak, N. E. Frattini, V. R. Joshi, A. Lingenfelter, S. Shankar, and M. H. Devoret, Kerr-free three-wave mixing in superconducting quantum circuits, Phys. Rev. Appl. **11**, 054060 (2019).

[40] A. Miano and O. A. Mukhanov, Symmetric traveling wave parametric amplifier, IEEE Trans. Appl. Supercond. **29**, 1501706 (2019).

[41] A. Fadavi Roudsari, D. Shiri, H. Renberg Nilsson, G. Tancredi, A. Osman, I. Svensson, M. Kudra, M. Rommel, J. Bylander, V. Shumeiko, and P. Delsing, Three-wave mixing traveling-wave parametric amplifier with periodic variation of the circuit parameters, Appl. Phys. Lett. **122**, 052601 (2023).

[42] H. Renberg Nilsson, A. Fadavi Roudsari, D. Shiri, P. Delsing, and V. Shumeiko, High-gain traveling-wave parametric amplifier based on three-wave mixing, Phys. Rev. Appl. **19**, 044056 (2023).

[43] A. G. Fox, S. E. Miller, and M. T. Weiss, Behaviour and applications of ferrites in the microwave region, Bell Syst. Tech. J. Bell Labs **34**, 5 (1955).

[44] B. Abdo, K. Sliwa, S. Shankar, M. Hatridge, L. Frunzio, R. Schoelkopf, and M. Devoret, Josephson directional amplifier for quantum measurement of superconducting circuits, Phys. Rev. Lett. **112**, 167701 (2014).

[45] B. Abdo, N. Bronn, O. Jinka, S. Olivadese, M. Brink, and J. Chow, Multi-path interferometric Josephson directional amplifier for qubit readout, Quantum Sci. Technol. **3**, 024003 (2018).

[46] Bekim Fazliji, Arpit Ranadive, Gwenael Legal, Giulio Cappelli, Guilliam Butseraen, Cécile Naud, Quentin Ficheux, Wiebke Guichard, Luca Planat, Olivier Buisson, and Nicolas Roch, Traveling wave parametric amplifiers with inbuilt reverse isolation, Part I, APS March Meet. **Z46**, 0004 (2024).

[47] Arpit Ranadive, Bekim Fazliji, Gwenael Legal, Giulio Cappelli, Guilliam Butseraen, Luca Planat, Cécile Naud, Quentin Ficheux, Wiebke Guichard, Olivier Buisson, and Nicolas Roch, Traveling wave parametric amplifiers with inbuilt reverse isolation, Part II, APS March Meet. **Z46**, 0005 (2024).

[48] Maxime Malnou, Benton T. Miller, José A. Estrada, Katarina Cicak, Kristen L. Genter, John D. Teufel, José Aumentado, and Florent Lecocq, TWPAC—The traveling-wave

parametric amplifier and converter: Design and characterization, APS March Meet. **Z46**, 0006 (2024).

[49] T. Dixon, J. W. Dunstan, G. B. Long, J. M. Williams, P. J. Meeson, and C. D. Shelly, Capturing complex behavior in Josephson traveling-wave parametric amplifiers, Phys. Rev. Appl. **14**, 034058 (2020).

[50] N. E. Frattini, U. Vool, S. Shankar, A. Narla, K. M. Sliwa, and M. H. Devoret, 3-wave mixing Josephson dipole element, Appl. Phys. Lett. **110**, 222603 (2017).

[51] G. L. Matthaei, L. Young, and E. M. T. Jones, *Microwave Filters, Impedance-Matching Networks, and Coupling Structures* (McGraw-Hill Book Company, Inc., Norwood, 1964).

[52] D. Shiri, H. Renberg Nilsson, P. Telluri, A. Fadavi Roudsari, V. Shumeiko, C. Fager, and P. Delsing, Modeling and harmonic balance analysis of parametric amplifiers for qubit read-out, ArXiv:2306.05177.

[53] T. Sweetnam, D. Banys, V. Gilles, M. A. McCulloch, and L. Piccirillo, Simulating the behaviour of travelling wave superconducting parametric amplifiers using a commercial circuit simulator, Supercond. Sci. Tech. **35**, 095011 (2022).

[54] K. Sundqvist, S. Kintas, M. Simoen, P. Krantz, M. Sandberg, C. Wilson, and P. Delsing, The pumpistor: A linearized model of a flux-pumped superconducting quantum interference device for use as a negative-resistance parametric amplifier, Appl. Phys. Lett. **103**, 102603 (2013).

[55] K. Sundqvist and P. Delsing, Negative-resistance models for parametrically flux-pumped superconducting quantum interference devices, EPJ Quantum Technol. **1**, 6 (2014).

[56] R. S. Engelbrecht and K. Kurokawa, A wide-band low noise L-band balanced transistor amplifier, Proc. IEEE **53**, 237 (1965).

[57] D. M. Pozar, *Microwave Engineering* (John Wiley & Sons, Inc., 2012).

[58] J. Butler and R. Lowe, *Beam-Forming Matrix Simplifies Design of Electronically Scanned Antennas* (Electronic Design, 1961), Vol. 9, pp. 170–173.

[59] Private Conversation with Vincent Desmaris.

[60] Swedish Patent Application 2351111-6.

[61] H. Rashid, D. Meledin, V. Desmaris, A. Pavolotsky, and V. Belitsky, Superconducting 4–8-GHz hybrid assembly for 2SB cryogenic THz receivers, IEEE Trans. Terahertz Sci. Technol. **4**, 193 (2014).

[62] F. Lecocq, L. Ranzani, G. A. Peterson, K. Cicak, A. Metelmann, S. Kotler, R. W. Simmonds, J. D. Teufel, and J. Aumentado, Microwave measurement beyond the quantum limit with a nonreciprocal amplifier, Phys. Rev. Appl. **13**, 044005 (2020).